Supplementary Information (SI) for Nanoscale.
This journal is © The Royal Society of Chemistry 2026

Electronic Supplementary Material

Dysprosium induced structure modulation for reduced working potential and enriched lithium storage sites

Yi Zhu,[a] Peng Li, [a,b,] Peng Zhao,[b] Yingchun Yan,[a] Qinggang Zhang,[a,*] Xinghui Liang,[c]*

Rongzhou Wang,[a,] Minghui Tan [d] and Mingbo Wu [d,e,*]*

[a.] *School of Chemistry and Chemical Engineering, Shandong University of Technology, Zibo, 255000, China.*

[b.] *Department of Physics and Astronomy, University of California, Irvine, CA, 92697, USA.*

[c.] *School of Metallurgy and Environment, Central South University, Changsha, 410083, China.*

[d.] *Department of Chemical Engineering, Qingdao University of Science and Technology, Qingdao, 266061, China.*

[e.] *Shandong Key Laboratory of Advanced Electrochemical Energy Storage Technologies, China University of Petroleum (East China), Qingdao, 266580, China.*

**Corresponding authors:*

Peng.Li.UPC@hotmail.com; zhangqg@sdut.edu.cn; rongzhouwang@sdut.edu.cn; wumb@qust.edu.cn

Table of Contents

Experimental Sections

1. Materials

All chemicals were used as received without further purification. N-methyl-2-pyrrolidinone (NMP) was bought from Aladdin. Lithium metal chips. tetrabutyl titanate ($C_{16}H_{36}O_4Ti$), hexahydrate nitric dysprosium ($Dy(NO_3)_3 \cdot 6H_2O$), monohydrate citric acid ($C_5H_8O_{10} \cdot H_2O$), sodium hydroxide (NaOH), ethanol (C_2H_5OH), and lithium nitrate ($LiNO_3$) were purchased from Energy Chemical. Ammonium hydroxide ($NH_3 \cdot H_2O$) was bought from Fuyu chemical. Lithium titanate was bought from Ningbo Lanli New Energy Technology. Poly(vinylidene fluoride) (PVDF), carbon black and the electrolyte (1M $LiPF_6$ in DEC:EC=1:1 Vol% with 10% FEC) was purchased from Duoduo Chemical company. Commercial lithium titanate (LTO) was obtained from Zhitian Nano-Micro New Material Co., Ltd.

2. Synthesis of sodium and lithium dysprosium titanate

Preparation of sodium dysprosium titanate (NADT): A homogeneous solution, designated as Solution A, was typically formed by dissolving 1.4 g of tetrabutyl titanate ($C_{16}H_{36}O_4Ti$), 1.5 g of dysprosium nitrate hexahydrate ($Dy(NO_3)_3 \cdot 6H_2O$), and 6.7 g of citric acid monohydrate ($C_5H_8O_{10} \cdot H_2O$) in 25 mL of ethanol under stirring, to which a sodium hydroxide solution (0.2 g of NaOH in 3 mL deionized water) was first added dropwise, and during which ammonium hydroxide ($NH_3 \cdot H_2O$) was then introduced dropwise under continuous stirring to adjust the pH to 7, resulting in the formation of a white gel-like precipitate. The gel solution was first dried in an oven at 80°C for 4 hours

to remove the solvent, followed by heating at 120°C for 12 hours to allow for polymerization. The resulting black product was then calcined in a furnace at 900°C for 1 hour, yielding the final sodium dysprosium titanate.

Preparation of lithium dysprosium titanate (LIDT)*:* The obtained sodium dysprosium titanate was subjected to an ion exchange process with a 50% excess of molten $LiNO_3$ at 350 °C for 4 hours, during which the product was subsequently washed with deionized water and dried in an oven, and this entire procedure was repeated in triplicate to achieve thorough replacement of sodium ions with lithium ions.

Preparation of LIMT (M= Rare earth element)*:* Fabrication of an analogous series of LIMT materials, where M represents various rare-earth elements (Ce, Nd, Eu, Tb and La), was carried out. The preparation steps were consistent with those previously outlined, with the only variation being that $Dy(NO_3)_3$ was substituted by an equivalent molar quantity of the corresponding rare-earth nitrate.

3. Materials characterization

The crystal structure of the synthesized material was examined by powder X-ray diffraction (XRD) using a Bruker D8 Advance diffractometer with Cu Kα radiation. Morphological analysis was performed by scanning electron microscopy (SEM) and high-resolution transmission electron microscopy (HRTEM). Energy-dispersive X-ray spectroscopy (EDS) mapping was performed on FEI-Talos F200S equipped with an EDS detector. Atomic-resolution high-angle annular dark-field (HAADF) imaging was conducted on a Thermo Scientific Themis Z microscope equipped with a double CEOS

probe corrector. Raman spectra were acquired on a HORIBA HR Evolution microscope with a 532 nm laser. UV-visible spectra were recorded using a Purkinje TU-1901 spectrophotometer. The sample surface chemistry was analyzed by X-ray photoelectron spectroscopy (XPS) on a Thermo Scientific ESCALAB instrument. Time-of-flight secondary ion mass spectrometry (TOF-SIMS) was performed using a PHI nanoTOF II instrument. For the in-situ XRD experiments, a custom cell with a beryllium window was employed to allow X-ray transmission. Patterns were collected at 10-minute intervals during galvanostatic discharge/charge cycles. The anode was fabricated by blending the active material, acetylene black, and polyvinylidene fluoride (PVDF) binder in an 8:1:1 mass ratio. The current density for the in-situ test was set at 50 mA g^{-1}.

4. Electrochemical measurements

CR2016-type coin cells were assembled to evaluate the electrochemical performance. The working electrode was prepared by mixing the active material, Super P, and PVDF binder (8:1:1 by weight) in NMP, and the resulting homogeneous slurry was cast onto a Cu foil. After drying at 80 °C for 12 h under vacuum, the electrode was punched into 12-mm disks, with the active material mass loading controlled at about 0.8 mg cm^{-2}. The cells were constructed in an argon-filled glove box using lithium foil as the counter electrode and a Celgard film as the separator. Before testing, the cells were aged for 8 hours to allow for thorough electrolyte wetting. All galvanostatic charge/discharge tests were carried out between 0.01 and 3.0 V (*vs*. Li^+/Li).

$LiFePO_4$/LIDT and $LiFePO_4$/LTO full cells were assembled with LIDT or commercial $Li_4Ti_5O_{12}$ as the anode and commercial $LiFePO_4$ as the cathode, respectively. The $LiFePO_4$ cathode was prepared by dispersing a mixture of the active material, acetylene black, and polyvinylidene fluoride (PVDF) binder at an 8:1:1 weight ratio in N-methyl-2-pyrrolidone (NMP) to form a slurry, cast onto an aluminum foil and dried at 80 °C for 12 hours under vacuum, prior to being punched into 12-mm-diameter disks for cell assembly. The specific capacity (C_t) of full-cell is calculated based on the supplementary equation (1):

$$C_t = \frac{I \times t}{m_a} \quad (1)$$

where t (h) represents the total time of the discharge, I (mA) is denoted as the current of the cell and m_a (kg) corresponds the mass of LIDT in the anode.

The galvanostatic intermittent titration technique (GITT) was utilized to quantify the Li^+ diffusion coefficient with a pulse current of 0.1 C for 30 min between 4 h rest intervals. The cyclic voltammetry (CV) measurements were conducted employing an Ivium-n-Stat electrochemical workstation, utilizing an identical electrode composition to the galvanostatic tests, and were scanned within the potential range of 0.01–3.0 V (*vs*. Li^+/Li).

5. DFT calculations

Calculations based on Density Functional Theory (DFT) first principles were performed *via* the Materials Studio Dmol3[1] and CASTEP[2] software package. Geometry optimization and energy calculations of the spin-polarized density functionals were

carried out using the generalized gradient approximation (GGA) of the Perdew-Burke-Ernzerhof (PBE). The positive and negative electrostatic potential regions were identified using the molecular electrostatic potential (MEP). Geometry optimizations were considered converged when the total energy change was below 10^{-5} eV and the maximum residual force on each atom was less than 0.01 eV $Å^{-1}$. Core electrons and the nuclei are described by the projector augmented wave method, and the plane-wave energy cutoff was set to 550 eV. The lattice volume and atom positions were fully relaxed until the total energy and maximum ionic Hellmann-Feynman forces acting was less than 10^{-10} eV and 10^{-4} eV/Å, respectively. The projected density of states (PDOS) of LIDT before and after lithiation were calculated using a Monkhorst−Pack grid of 11 × 25 × 25 k-points. For pristine LIDT, there are eight possible positions to accommodate Li atoms, which has been proved by the crystal structure refinement from the neutron diffraction patterns[3]. The formation energy of Li interstitial was calculated by the equation:

$$E = \frac{E_{\text{lithiated}} - E_{\text{pristine}} - 8E_{\text{Li}}}{8} \tag{2}$$

where the $E_{\text{lithiated}}$ and E_{pristine} are the total energy of lithiated LIDT and pristine LIDT, respectively, and E_{Li} is the energy of a single Li atom in bulk Li of bcc phase.

Supporting Figures

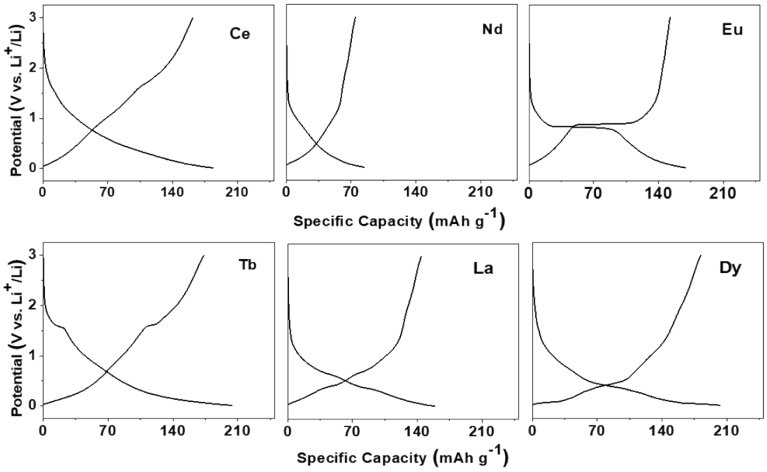

Figure S1 Voltage profile of the LIMT electrode during the second charge-discharge cycle at 0.1 C.

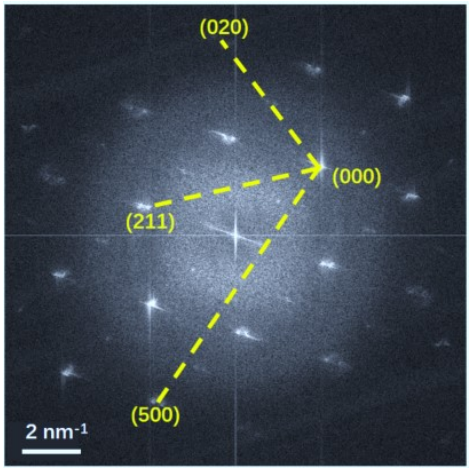

Figure S2. FFT image of the prepared LIDT.

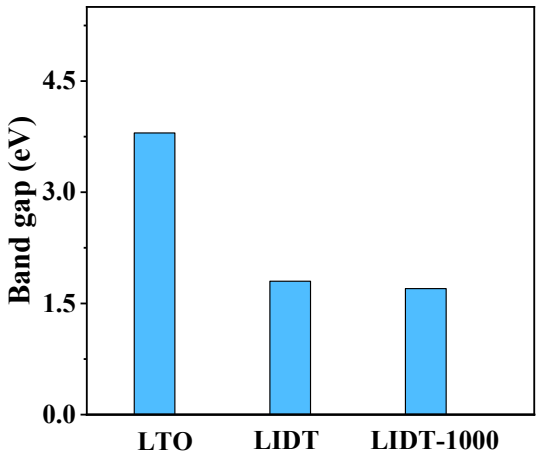

Figure S3 Band gap of LTO, LIDT and LIDT-1000

The energy band gap of the active material is calculated based on the Kubelka-Munk equation.[4]

$$(ahv)^{n} = c(hv - E) \quad (3)$$

where α, h, v, c are absorption coefficients, Planck constants, frequencies and constants, respectively. The introduction of Dy reduces the bandgap of LTO, and the concomitant formation of oxygen vacancies can significantly enhance carrier density and electronic conductivity, thereby improving the rate performance.

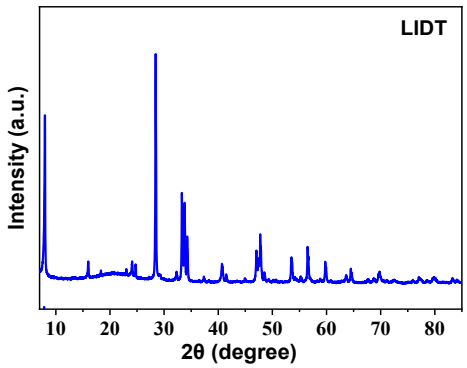

Figure S4 XRD pattern of LIDT

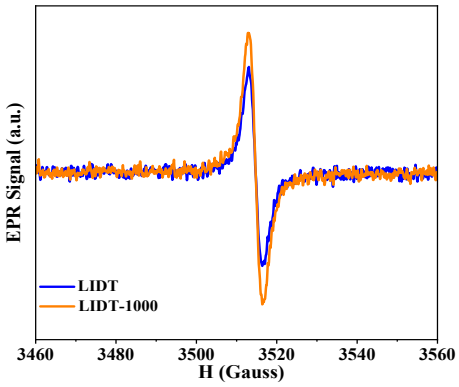

Figure S5 EPR profiles of the original LIDT and the LIDT after 1000 cycles.

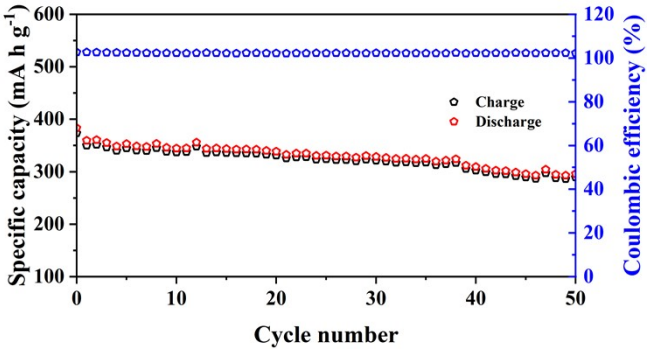

Figure S6 Cycling performance of the LIDT electrode at a high mass loading of ~2.0 mg cm^{-2}.

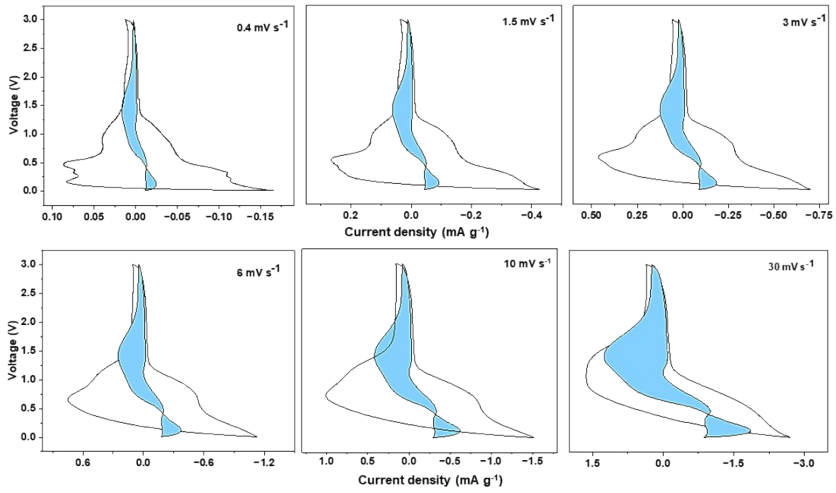

Figure S7 CV curves of the capacitive contribution of LIDT at 0.4, 1.5, 3, 6, 10 and 30 mV s^{-1}

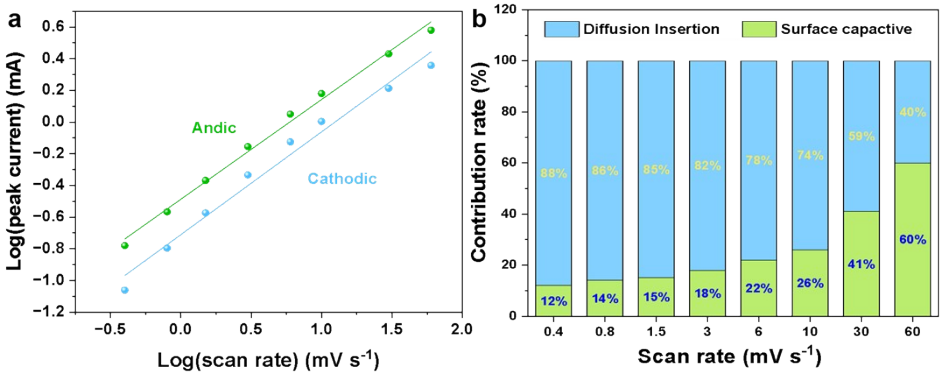

Figure S8 (a) The linear relationship between log (*i*, peak current) and log (*v*, scan rate). (b) The percentages of the capacitive and diffusion contributions.

To elucidate the electrochemical kinetics of the LIDT electrode, cyclic voltammetry (CV) was performed at various scan rates, and the correlation between the peak current (*i*) and the scanning rate (v) can be described by the following formula: [5]

$$i_{(v)} = av^b \tag{4}$$

where *a* and *b* represent tunable parameters. The value of *b* can be determined by analyzing the log(*i*)–log(*v*) relationship using the equation provided below:

$$\log i_{(v)} = b\log v + \log a \tag{5}$$

specifically, the value of *b* can be derived from the slope of Equation (5). A *b* value of 0.5 indicates a fully diffusion-controlled process, whereas a *b* value of 1 signifies a purely capacitive contribution. The linear correlation between log(i) and log(v) presented in Figure S6a yields b-values of 0.65 and 0.63, derived from the anodic and cathodic peaks respectively, suggesting that the energy storage mechanism in lithium-ion batteries is predominantly governed by a diffusion-controlled process. Based on

Dunn's theory, the contributions of capacitor-like (k_1v) and diffusion-controlled ($k_2v^{1/2}$) charge storage can be separated using the following equation:[6]

$$i_{(v)}/v^{1/2} = k_1v^{1/2} + k_2 \quad (6)$$

where the response current i at a certain potential can be divided into two components originated from capacitive effects and diffusion-controlled reactions, respectively. The constants k_1 and k_2 in the above equations are constants to a given potential and can be determined from the linear relationship between $i_{(V)}/v^{1/2}$ and $v^{1/2}$, where k_1 represents the slope and k_2 denotes the y-intercept. Capacitive contributions at predetermined scan rates are computable using this established protocol. For example, the capacitive proportion is approximately 14% at a scan rate of 0.8 mV s^{-1} (Figure S6b).

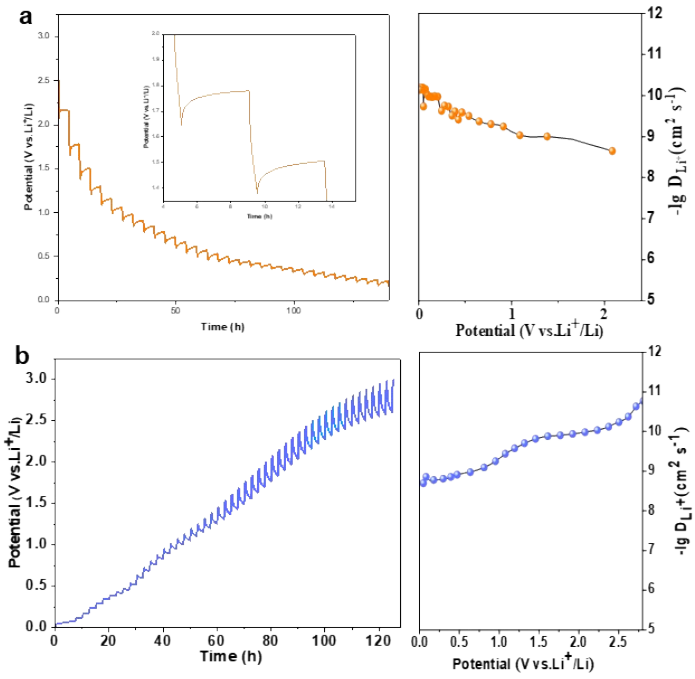

Figure S9 GITT curves and calculated Li^+ diffusion coefficients of LIDT electrodes.

To ascertain the diffusion coefficients of Li^+ ions (D_{Li+}), the galvanostatic intermittent titration technique (GITT) measurement was additionally performed (Figure S7). D_{Li+} was computed based on Fick's second law.[7]

$$D_{Li^+} = \frac{4}{\pi\tau}\left(\frac{n_m v_m}{s}\right)^2\left(\frac{\Delta E_s}{\Delta E_t}\right) \tag{7}$$

in the equation, τ represents the duration of the current pulse, S denotes the contact area between the electrode and the electrolyte (cm^2), n_m and V_m stand for the moles (mol) and molar volume (cm^3 mol^{-1}) of the active material, ΔE_s indicates the potential difference between the two equilibrium potentials, and ΔE_t represents the potential difference during the constant current pulse.

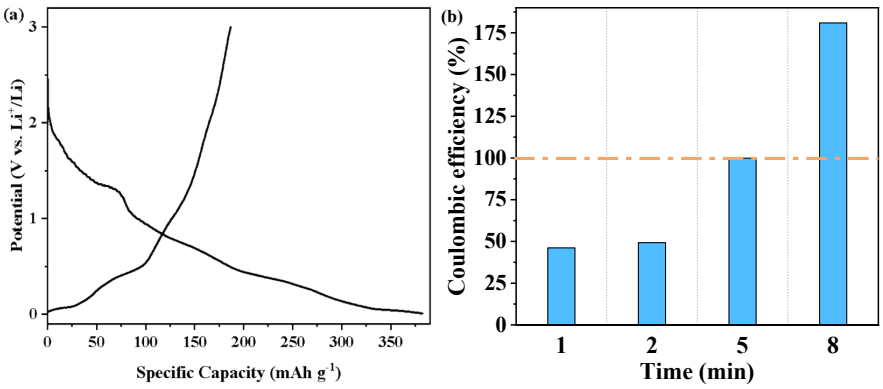

Figure S10 (a) The initial discharge-charge profile at 0.1 C of LIDT. (b) Dependence of the ICE on prelithiation time.

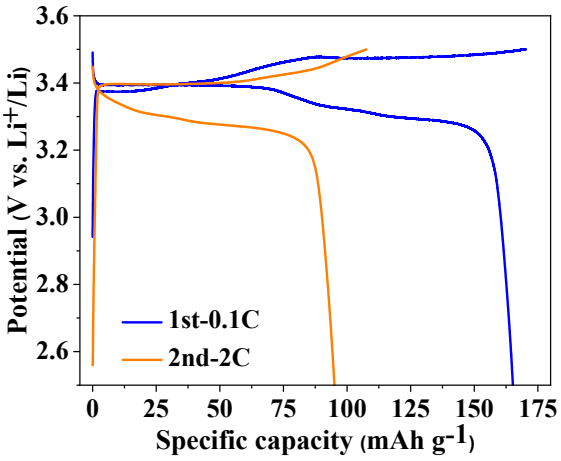

Figure S11 Discharge-charge profiles at 0.1 C and 2 C

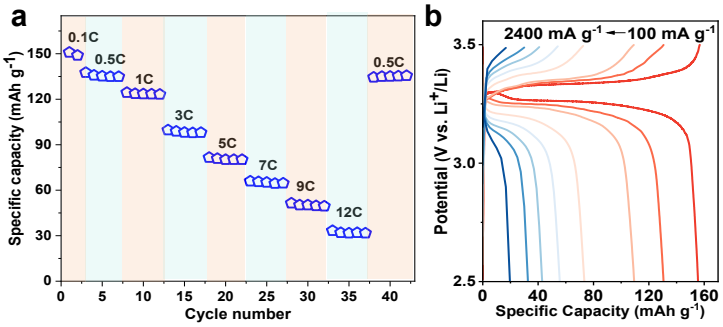

Figure S12 (a) Rate capability of the $LiFePO_4$/LIDT full cell. (b) Discharge-charge profile of LIDT at different current densities.

Supporting Tables

Table S1. Rietveld refinement results of LIDT.

Rwp=6.68%, Rp=5.13%					
Pbcm a=11.12 Å,b=5.39 Å and c=5.39 Å, α=β=γ=90°					
Atom	Wyckoff	x	y	z	Occupancy
Li	4d	0.512	0.250	0	1
Dy	4d	0.881	0.204	0.250	1
Ti	4d	0.288	0.016	0.250	1
O(1)	4c	0.240	0.250	0	1
O(2)	4c	0.746	0.250	0	1
O(3)	4d	0.085	-0.063	0.250	1
O(4)	4d	0.459	-0.006	0.250	1

Table S2. The reported electrochemical properties of the Ti-based anode materials.

Materials	Working potential	Specific capacity	Current density	Cycling life	Ref.
$TiNbO_7$	1.66 V	281 mAh g^{-1}	1C	1000 cycles	[8]
Li_2TiSiO_5/EG	0.43 V	190 mAh g^{-1}	200 mA g^{-1}	100 cycles	[9]
Li_2TiSiO_5@C	0.28 V	172 mAh g^{-1}	500 mA g^{-1}	1000 cycles	[9]
Li_2TiGeO_5	0.5 V	406 mAh g^{-1}	1 A g^{-1}	600 cycles	[10]
$La_{0.5}Li_{0.5}TiO_3$	1 V	<100 mAh g^{-1}	10 C	3000 cycles	[11]
Na_2TiGeO_5	0.8 V	309 mAh g^{-1}	0.5 A g^{-1}	4000 cycles	[12]
Na_2TiSiO_5	0.8 V	188 mAh g^{-1}	0.5 A g^{-1}	300 cycles	[13]
$La_{0.54}Li_{0.27}TiO_{2.945}$	1 V	145 mAh g^{-1}	--	50 cycles	[14]
$LiEuTiO_4$	0.8 V	217mAh g^{-1}	100 mA g^{-1}	500 cycles	[15]
$Li_4Ti_5O_{12}$	1.5 V	155 mAh g^{-1}	50 C	2000 cycles	[16]
$LiYTiO_4$	0.3 V	125 mAh g^{-1}	20 C	3000 cycles	[17]
$Li(V_{0.5}Ti_{0.5})S_2$	0.9 V	205mAh g^{-1}	0.5 C	100 cycles	[18]
LIDT	0.5	150 mAh g^{-1}	20 C	4500 cycles	this work

Supporting References

1. S. Wang, S. Tian, Y. He, B. Zheng, H. Xiong, L. Li, H. Li, Y. Wang and L. Tang, *Separation and Purification Technology*, 2025, **364**.
2. D. Liu, J. Deng and Y. Jin, *Applied Surface Science*, 2014, **290**, 35-39.
3. S.-H. Song, K. Ahn, M. G. Kanatzidis, J. A. Alonso, J.-G. Cheng and J. B. Goodenough, *Chemistry of Materials*, 2013, **25**, 3852-3857.
4. G. Li, Z. Zhang, H. Peng and K. Chen, *RSC Advances*, 2013, **3**, 11507-11510.
5. J. Li, J. K. El‐Demellawi, G. Sheng, J. Björk, F. Zeng, J. Zhou, X. Liao, J. Wu, J. Rosen, X. Liu, H. N. Alshareef and S. Tu, *Energy & Environmental Materials*, 2024, **7**.
6. Q. Wei, T. Huang, X. Huang, B. Wang, Y. Jiang, D. Tang, D. L. Peng, B. Dunn and L. Mai, *Interdisciplinary Materials*, 2023, **2**, 434-442.
7. X. Hao and B. M. Bartlett, *Advanced Energy Materials*, 2013, **3**, 753-761.
8. B. Guo, X. Yu, X.-G. Sun, M. Chi, Z.-A. Qiao, J. Liu, Y.-S. Hu, X.-Q. Yang, J. B. Goodenough and S. Dai, *Energy Environ. Sci.*, 2014, **7**, 2220-2226.
9. J. Liu, W. K. Pang, T. Zhou, L. Chen, Y. Wang, V. K. Peterson, Z. Yang, Z. Guo and Y. Xia, *Energy & Environmental Science*, 2017, **10**, 1456-1464.
10. Y. Liu, Q. Bai, A. M. Nolan, Y. Zhou, Y. Wang, Y. Mo and Y. Xia, *Nano Energy*, 2019, **66**.
11. L. Zhang, X. Zhang, G. Tian, Q. Zhang, M. Knapp, H. Ehrenberg, G. Chen, Z. Shen, G. Yang, L. Gu and F. Du, *Nat Commun*, 2020, **11**, 3490.
12. Z. Liu, D. He, B. Wang, T. Wu, S. Zhao, X. Li, S. He, Y. Liang, Y. Zhou, S. Sun and H. Yu, *Small*, 2022, **18**, e2107608.
13. D. He, T. Wu, B. Wang, Y. Yang, S. Zhao, J. Wang and H. Yu, *Chem Commun (Camb)*, 2019, **55**, 2234-2237.
14. C. Hua, X. Fang, Z. Wang and L. Chen, *Electrochemistry Communications*, 2013, **32**, 5-8.
15. J. Huang, K. Yang, Z. Zhang, L. Yang and S. I. Hirano, *Chem Commun* 2017, **53**, 7800-7803.
16. D. Wang, H. Liu, M. Li, X. Wang, S. Bai, Y. Shi, J. Tian, Z. Shan, Y. S. Meng, P. Liu and Z. Chen, *Energy Storage Materials*, 2019, **21**, 361-371.
17. Y. Zhang, J. Huang, N. Saito, X. Yang, Z. Zhang, L. Yang and S. i. Hirano, *Advanced Energy Materials*, 2022, **12**.
18. S. J. Clark, D. Wang, A. R. Armstrong and P. G. Bruce, *Nat Commun*, 2016, **7**, 10898.